Density Functional Theory (DFT) and DRIFTS Investigations of the Formation and Adsorption of Enolic Species on the Ag/Al_2O_3 Surface

Hongwei Gao, Hong He,* Yunbo Yu, and Qingcai Feng

Research Center for Eco-Environmental Sciences, Chinese Academy of Sciences, Beijing, 100085, China

Received: February 24, 2005; In Final Form: May 10, 2005

Molecular structure and vibrational frequencies of the novel surface enolic species intermediate on Ag/Al_2O_3 have been investigated by means of density functional theory (DFT) calculations and in situ infrared spectroscopy. The geometrical structures and vibrational frequencies were obtained at the B3P86 levels of DFT and compared with the corresponding experimental values. Theoretical calculations show that the calculated IR spectra are in good agreement with the experimental spectroscopic results. In addition, the adsorption energy of enolic species on the Ag/Al_2O_3 catalyst surface was also evaluated. The reaction mechanism from C_2H_5OH to enolic species on Ag/Al_2O_3 catalyst was proposed.

1. Introduction

The alumina supported silver catalyst (Ag/Al_2O_3) has been studied as a promising catalyst due to its high activity for the selective catalytic reduction (SCR) of NO_x by hydrocarbons in the presence of excess oxygen.[1−3] In particular, C_2H_5OH is extremely effective for the SCR of NO_x over Ag/Al_2O_3.[3] On the basis of these studies, a possible mechanism for the SCR of NO_x by C_2H_5OH over Ag/Al_2O_3 was considered as similar to that of C_3H_6, approximately, $NO + O_2 + C_2H_5OH \rightarrow NO_x$ (nitrate in particular) + $C_xH_yO_z$ (acetate in particular) → R-NO_2 + R-ONO → −NCO + −CN + NO + $O_2 \rightarrow N_2$.[4,5] However, this mechanism does not sufficiently explain why C_2H_5OH has a higher efficiency for the SCR of NO_x over Ag/Al_2O_3 than C_3H_6.[6]

Recently, we found a novel surface species on the Ag/Al_2O_3 surface during the partial oxidation of C_2H_5OH, which was assigned to an enolic species ($CH_2{=}CH{-}O^-$) based on the feature of 1633, 1416, and 1336 cm^{-1} shown in the in situ FTIR.[3] The enolic species has been suggested as an important reaction intermediate that relates to the higher efficiency for the SCR of NO_x with C_2H_5OH as a reductant.[6] One evidence is that the IR spectra of *syn*-vinyl alcohol ($CH_2{=}CHOH$) in the gas phase show a strong peak between 1644 and 1648 cm^{-1}, which is accompanied by two peaks at 1409−1412 and 1300−1326 cm^{-1}.[7−10] However, no IR data of an enolic species have been reported on the adsorbed status. Therefore, we have no experimental evidence to directly support our assignment of surface enolic species.

Auxiliary computer simulation of IR spectra with density functional theory (DFT) quantum mechanical methods affords highly powerful and reliable tools for analytical chemistry by means of in situ Diffuse Reflectance Infrared Fourier Transform Spectroscopy (DRIFTS). Due to the use of IR simulations, impressive advances have been achieved in separation and unambiguous identification of complex mixtures of organic compounds. The most efficient is especially for the analysis of unknown compounds. DFT calculations are increasingly being applied to predict the interactions of adsorbates with catalytic sites.[11] Such DFT methods provided accurate geometries, and reasonable energetics for molecules containing transition metals[12−15] are sufficient to describe the active sites in comparison of the predictions with experimental data.

The objective of this work is to study the adsorbed enolic species on the Ag/Al_2O_3 catalyst with experimental and theoretical methods. This study aims to utilize in situ FTIR spectroscopies and simulant ones toward the understanding of the formation of these active sites on the Ag/Al_2O_3 catalyst and their involvement in the reaction mechanism of the SCR of NO_x. The fundamental understanding of the reaction mechanism of the SCR of NO_x is believed to be essential for the development of the catalyst and improvement for potential application.

2. Computational Section

Minimum energy structure and normal mode calculations were performed for ten calculated models with the Gaussian98 program. The properties of the calculated models were determined through the application of density functional theory (DFT), using the B3P86 gradient corrected function (Becke's 3-parameter function with the nonlocal correlation provided by the Perdew 86 expression). The LANL2DZ effective core potential basis set was used for all of the calculations. The LANL2DZ basis replaced the 1s through 2p electrons of the heavy atoms with a potential field for a considerable computational savings. A double-ζ quality Dunning basis was used for the light atoms and the remaining heavy atom electrons. Stability calculations confirmed the ground-state configuration of all the wave functions. The calculated vibration frequencies and infrared intensity of the vibrational normal modes with Gaussian98 are picked up by the Hyperchem Version 6.0 package.

3. Experimental Section

The Ag/Al_2O_3 catalyst (Ag loading is 5.0 wt %) was prepared by an impregnation of γ-Al_2O_3 powder (200 m^2/g) with an appropriate amount of silver nitrate aqueous solution. The sample was dried at 393 K for 3 h and calcined at 873 K for 3 h in air.

In situ Diffuse Reflectance Infrared Fourier Transform Spectroscopy (DRIFTS) spectra were recorded with a Nexus

* Corresponding author. Phone: +86-10-62849123. Fax: +86-10-62923563. E-mail: honghe@mail.rcees.ac.cn.

10.1021/jp050955+ CCC: $30.25
Published on Web 06/16/2005

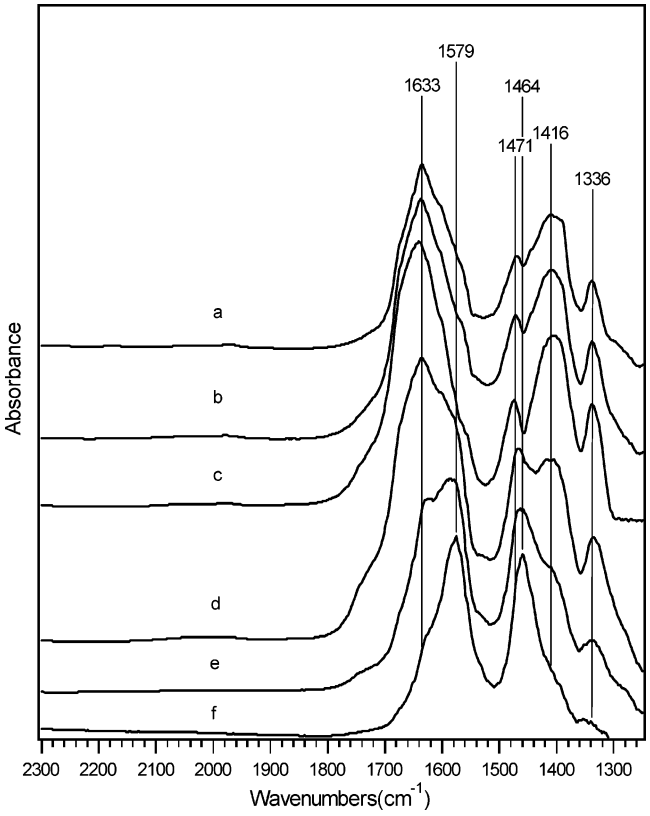

Figure 1. The experimental in situ DRIFTS spectra of adsorbed species in steady states on Ag/Al_2O_3 in a flow of $C_2H_5OH + O_2$ at (a) 473, (b) 523, (c) 573, (d) 673, (e) 773, and (f) 873 K. Conditions: C_2H_5OH 1565 ppm, O_2 10%.

670 (Thermo Nicolet) FT-IR, equipped with an in situ diffuse reflection chamber and a high-sensitivity MCT detector. The Ag/Al_2O_3 catalyst for the in situ DRIFTS studies was finely ground and placed into a ceramic crucible in the in situ chamber. Mass flow controllers and a sample temperature controller were used to simulate the real reaction conditions, such as mixture of gases, pressure, and sample temperature. Prior to recording each DRIFTS spectrum, the sample was heated in situ in 10% O_2/N_2 flow at 873 K for 1 h, then cooled to the desired temperature befor taking a reference spectrum. All gas mixtures were fed at a flow rate of 100 mL/min. All spectra were measured with a resolution of 4 cm^{-1} and with an accumulation of 100 scans.

4. Results and Discussion

4.1. Experimental Results. Figure 1 shows the in situ DRIFTS of Ag/Al_2O_3 in a flow of C_2H_5OH (1565 ppm) + O_2 (10%) at a temperature range of 473−873 K in steady states. Exposure of this catalyst to the fed gas at 473 K resulted in the appearance of five peaks (1633, 1579, 1471−1464, 1416, and 1336 cm^{-1}). Peaks at 1579 and 1471−1464 cm^{-1} were assigned to ν_{as}(OCO) and ν_s(OCO) of acetate, respectively.[16−22] According to our earlier studies,[3] peaks at 1633, 1416, and 1336 cm^{-1} were assigned to asymmetric stretching vibration, symmetric stretching vibration, and C−H deformation vibration modes of an adsorbed enolic species, respectively. Apparently, the enolic species is predominant during the oxidation of C_2H_5OH on the Ag/Al_2O_3 surface within a low-temperature range of 473−673 K. However, the surface acetate species becomes dominant at a high-temperature range of 773−873 K.

4.2. Computational Results. *4.2.1. Calculation Models.* In our earlier study,[3] we proposed that the peak at 1633 cm^{-1} would be associated with the frequency of double bond stretching vibration, such as ν(C═C) and ν(C═O). In general, however, stretching vibration frequencies of isolated C═C and C═O should be higher than 1633 cm^{-1}. It should be noted that the IR spectra of gas-phase phenol and methoxy ethene give peaks between 1600 and 1650 cm^{-1},[7] as do the IR spectra of adsorbed catechol on a TiO_2 colloid and chemisorbed acetone−oxygen mixtures on nickel oxide.[5,24] Their common characteristic is an enolic structure. In this study, we conjectured that an enolic anion $R_2C{=}CH{-}O^-$ was formed during this process. The conjugation of the $R_2C{=}CH{-}O^-$ group may induce the vibrational mode of C−C−O to shift to a frequency lower than ν(C═C) and ν(C═O).[3,5,7,23] Moreover, the peaks of CH_3CHO (*m*/*z* 29), $CH_3CH{=}CH^+$ (*m*/*z* 41), $CH_2{=}CHCHO$ (*m*/*z* 56), and $CH_2{=}CH{-}CH{=}CH{-}OH$ (*m*/*z* 70) fractions originating from the thermal decomposition of the enolic species were observed in TPD spectra.[24] Therefore, we designed the calculated models containing two, three, and four carbon backbones (see Figure 2) to study the mechanism of enolic species adsorption on the Ag/Al_2O_3 cluster.

4.2.2. Mechanism for the Formation of Absorbed Enolic Species over Ag/Al_2O_3 Catalyst. During the partial oxidation of C_2H_5OH over Ag/Al_2O_3 at 473−873 K, peaks at 1633, 1416, and 1336 cm^{-1} were observed, moreover, these peaks predominate (shown in Figure 1), indicating that enolic species are the main surface species. In TPD-MS,[24] the peaks of CH_3CHO- (*m*/*z* 29) and $CH_2{=}CH{-}CH{=}CH{-}OH$ (*m*/*z* 70) fraction are the main peaks. On the basis of DRIFTS (Figure 1) and TPD-MS,[24] we proposed the mechanism for the formation of absorbed enolic species $(CH_2{=}CHO^-){-}M^+$, $(CH_2{=}CHCH_2{-}O^-){-}M^+$, and $(CH_2{=}CH{-}CH{=}CH{-}O^-){-}M^+$ over the Ag/Al_2O_3 catalyst as follows:

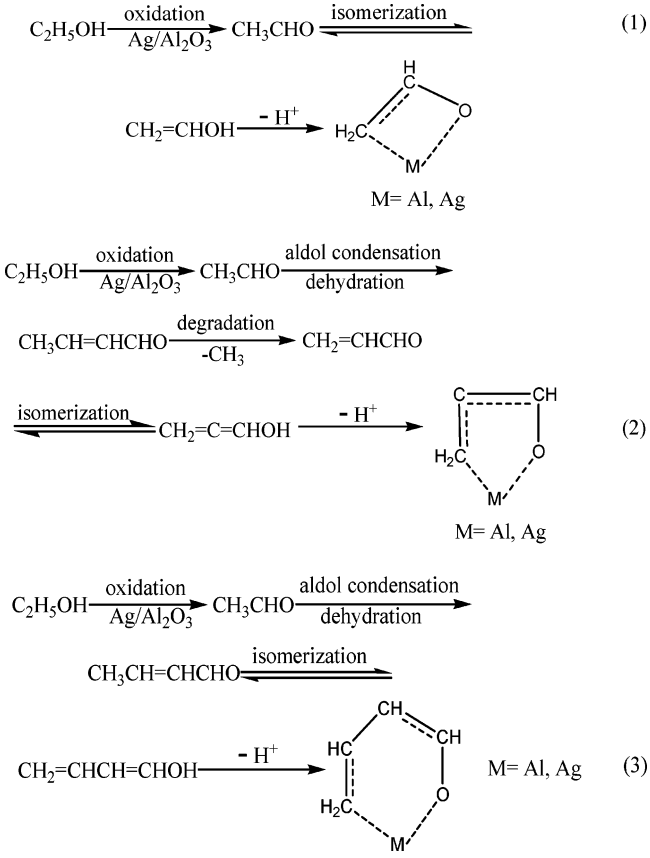

For reaction 1, C_2H_5OH is first catalytically oxidized to CH_3-CHO, then isomerizes and dehydrogenates to yield ($CH_2{=}CH{-}$

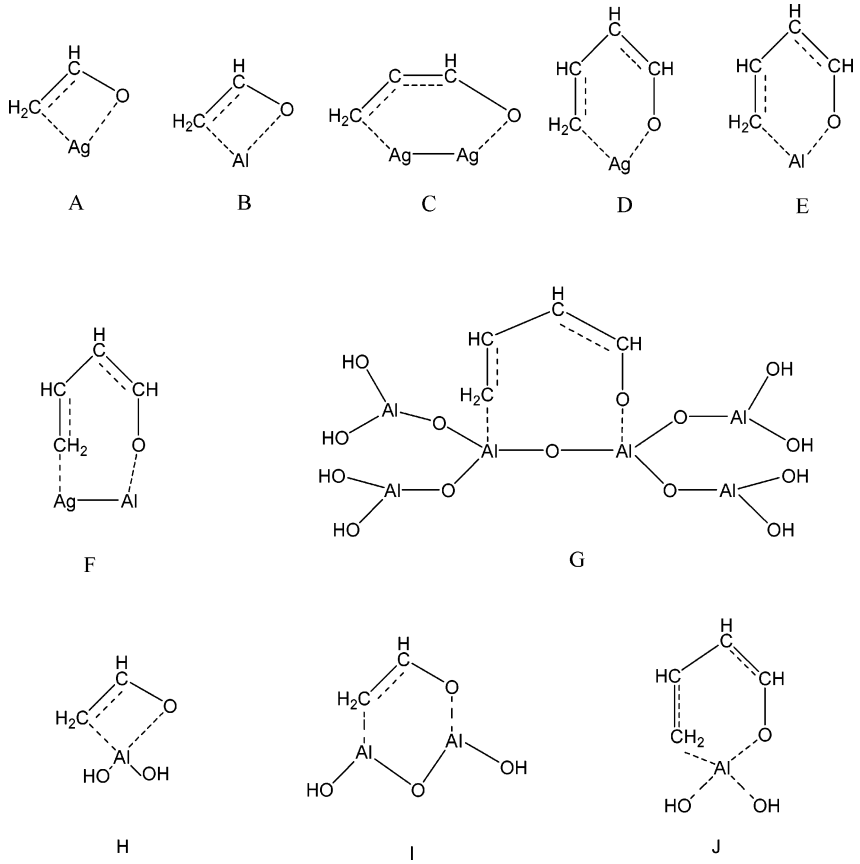

Figure 2. Calculated models for the reaction of enolic species on Ag/Al_2O_3 catalyst.

$O^-)-M^+$. For reaction 2, C_2H_5OH is first oxidized to CH_3CHO, which then condensates and dehydrogenates to yield $CH_3CH{=}CHCHO$, followed by degradation and isomerization to $CH_2{=}C{=}CHOH$ compound, and a further reaction of this compound finally leads to the formation of $(CH_2{=}C{=}CH{-}O^-){-}M^+$. The mechanism of reaction 3 is similar to that of reaction 2.

4.2.3. Vibrational Frequency Calculation. Structural optimizations and vibrational frequency calculation for models A−J were carried out at B3P86/LANL2DZ. Calculated frequencies are listed in Table 1. Simulant spectra for models A−J are shown in Figures 3−5.

The calculated antisymmetric stretching vibrational modes of the adsorbed enolic species for models A−J are 1645, 1693, 1505, 1599, 1694, 1654, 1597, 1694, 1900, and 1571 cm^{-1}, respectively (Figures 3−5). In comparison with the same experimental frequency of 1633 cm^{-1}, the error is on average about 12 cm^{-1} for model A, 60 cm^{-1} for model B, −128 cm^{-1} for model C, −34 cm^{-1} for model D, 61 cm^{-1} for model E, 21 cm^{-1} for model F, −36 cm^{-1} for model G, 61 cm^{-1} for model H, 267 cm^{-1} for model I, and −62 cm^{-1} for model J. The calculated frequencies of model A at 1645 cm^{-1} with 314 km/mol intensity and model F at 1654 cm^{-1} with 61 km/mol intensity in Figures 3 and 4 are relatively good matches of the most intense bands at 1633 cm^{-1} in the experimental spectrum (Figure 1).

The calculated symmetric stretching vibrational modes of the adsorbed enolic species for the models A−J are 1429, 1446, 1344, 1531, 1438, 1431, 1406, 1449, 1447, and 1406 cm^{-1}, respectively (Figures 3−5). For the same experimental frequency of 1416 cm^{-1}, overestimation of experimental frequency values is about 0.92% for model A, 2.12% for model B, 8.12% for model D, 1.55% for model E, 1.06% for model F, 2.33% for model H, and 2.18% for model I; underestimation of experimental frequency values is about 0.71% for models G and J. The symmetric stretching vibrational mode of the adsorbed enolic species of model A calculated at 1429 cm^{-1} with 68 km/

TABLE 1: Calculated Vibrational Frequencies (cm^{-1}) at the B3P86/LANL2DZ Level for the Ten Calculated Models

model	freq (cm^{-1})	intensity (km/mol)	experiment (cm^{-1})	vibration mode
A	1645	314	1633	enolic species a-str
	1429	67	1416	enolic species a-str
	1328	16	1336	C−H def
B	1693	246	1633	enolic species a-str
	1446	50	1416	enolic species str
	1264	320	1336	C−H def
C	1505	6	1633	enolic species a-str
	1344	28	1416	enolic species str
	1262	145	1336	C−H def
D	1599	104	1633	enolic species a-str
	1531	279	1416	enolic species str
	1370	78	1336	C−H def
E	1694	127	1633	enolic species a-str
	1438	55	1416	enolic species str
	1362	86	1336	C−H def
F	1654	61	1633	enolic species a-str
	1431	20	1416	enolic species str
	1347	53	1336	C−H def
G	1597	408	1633	enolic species a-str
	1406	120	1416	enolic species str
	1138	648	1336	C−H def
H	1694	275	1633	enolic species a-str
	1449	61	1416	enolic species str
	1375	87	1336	C−H def
I	1900	229	1633	enolic species a-str
	1447	17	1416	enolic species str
	1368	56	1336	C−H def
J	1571	139	1633	enolic species a-str
	1406	57	1416	enolic species str
	1377	17	1336	C−H def

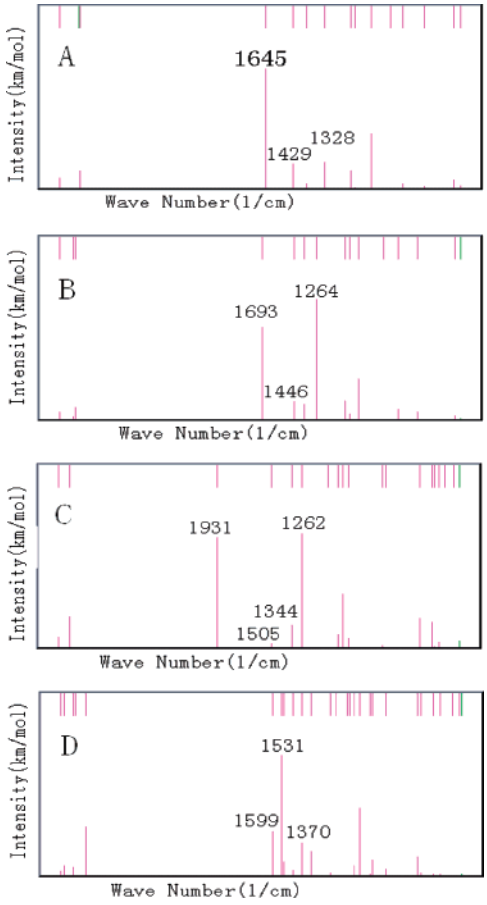

Figure 3. Calculated vibrational IR spectra for the models A, B, C, and D at the DFT-B3P86/LANL2DZ level.

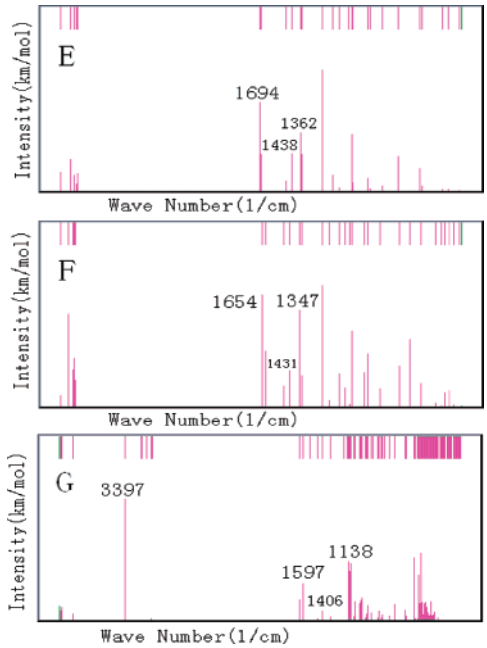

Figure 4. Calculated vibrational IR spectra for the models E, F, and G at the DFT-B3P86/LANL2DZ level.

mol intensity is only 13 cm^{-1} higher than the experimental spectrum at 1416 cm^{-1} with strong absorbance within 0.92% error. The symmetric stretching vibrational mode of the adsorbed enolic species of models G and J calculated at 1406 cm^{-1} is only 10 cm^{-1} lower than the experimental spectrum at 1416 cm^{-1} with strong absorbance within 1.06% error. The expressed

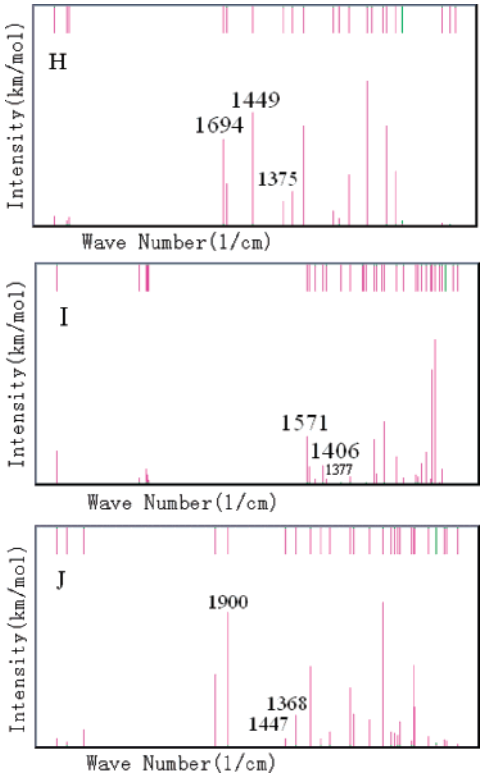

Figure 5. Calculated vibrational IR spectra for the models H, I, and J at the DFT-B3P86/LANL2DZ level.

frequency at 1429 cm^{-1} for model A in Figure 3 and that at 1406 cm^{-1} for models G and J in Figure 4 are relatively good matches of the most intense bands at 1416 cm^{-1} in the experimental spectrum (Figure 1).

The calculated C−H deformation vibrational modes of the adsorbed enolic species for the models A−J are 1328, 1264, 1262, 1370, 1362, 1347, 1138, 1375, 1368, and 1377 cm^{-1}, respectively (Figures 3−5). In comparison with the same experimental frequency of 1336 cm^{-1}, the error is on average about −8 cm^{-1} for model A, −72 cm^{-1} for model B, −74 cm^{-1} for model C, 34 cm^{-1} for model D, 26 cm^{-1} for model E, 11 cm^{-1} for model F, −198 cm^{-1} for model G, 39 cm^{-1} for model H, 32 cm^{-1} for model I, and 41 cm^{-1} for model J. The calculated spectra of model A at 1328 cm^{-1} with 16 km/mol intensity and model F at 1347 cm^{-1} with 53 km/mol are similar to the experimental spectrum at 1336 cm^{-1} with strong absorbance. The expressed frequency at 1328 cm^{-1} for model A in Figure 3 and that at 1347 cm^{-1} for model F in Figure 4 are relatively good matches of the most intense bands at 1336 cm^{-1} in the experimental spectrum (Figure 1).

Comparison with the experimental data shows that the spectra of models A and F simulated by DFT-B3P86 evidently best match the experimental counterparts for the overwhelming majority of the calculated models A−J considered in the present study.

4.2.4. Adsorption Energy. The adsorption energies (E_{ads}) in the present study are deduced by

$$E_{ads} = E_{cluster/adsorbate} - E_{cluster} - E_{adsorbate} \quad (4)$$

where $E_{cluster/adsorbate}$ is the total energy of the adsorbate on the cluster, $E_{cluster}$ is the total energy of the bare cluster (Ag/Al_2O_3 catalyst), and $E_{adsorbate}$ is the energy of the adsorbate (enolic species).

The calculated E_{ads} of models A−J are −180.77, −204.92, −158.82, −186.10, −196.43, −184.40, −106.85,−154.81,

−137.35, −157.88 kcal/mol, respectively. The negative E_{ads} values indicate that the adsorbed state (cluster/adsorbate) is energetically favorable. On the basis of the entire comparison of the E_{ads} values, it is clear that the order of the energetic stability of the adsorption states of the enolic species on the Ag/Al_2O_3 catalyst surface can be described as model B > model E > model D > model F > model A > model C > model J > model H > model I > model G. We conjecture that models B and E are more favorable on thermodynamics, but the formation of those structures is forbidden on dynamics. All models have big E_{ads} value, therefore, we consider that the enolic species easily formed on the Ag/Al_2O_3 catalyst surface.

5. Conclusions

Simulating infrared spectra with the density functional theory (DFT) method can be considered as an advantageous auxiliary tool for the FTIR identification of unambiguous compounds. The calculations show clearly that the calculated IR spectra for models A and F are of reasonable similarity to the corresponding experimental one. We conclude that models A and F are the reasonable models for the enolic species adsorption on the Ag/Al_2O_3 surface. The result of the adsorption energy shows that enolic species easily adsorbed on the Ag/Al_2O_3 catalyst surface.

Acknowledgment. This work was financially supported by the Innovation Program of the Chinese Academy of Sciences (KZCX3-SW-430) and the State Hi-tech Research and Development Project of the Ministry of Science and Technology, Peoples Republic of China (Grant 2003AA643010).

References and Notes

(1) Miyadera, T.; Yoshida, K. *Chem. Lett*. **1993**, 1483.
(2) Sumiya, S.; He, H.; Abe, A.; Takezawa, N.; Yoshida, K. *J. Chem. Soc., Faraday Trans.* **1998**, *94*, 2217.
(3) Yu, Y.; He, H.; Feng Q. *J. Phys. Chem. B* **2003**, *107*, 13090.
(4) Burch, R.; Breen, J. P.; Meunier, F. C. *Appl. Catal. B* **2002**, *39*, 283.
(5) Meunier, F. C.; Zuzaniuk, V.; Breen, J. P.; Olsson, M.; Ross, R. H. *Catal. Today* **2000**, *59*, 287−304
(6) Yu, Y.; He, H.; Feng, Q.; Gao, H.; Yang, X. *Appl. Catal. B* **2004**, *49*, 159.
(7) Standard IR Spectra, Sadtler Research Labs.
(8) Rodler, M.; Blom, C. E.; Bauder, A. *J. Am. Chem. Soc.* **1984**, *106*, 4029.
(9) Koga, Y.; Nakanaga, T.; Sugawara, K.; Watanabe, A.; Sugie, M.; Takeo, H.; Kondo, S.; Matsumura, C. *J. Mol. Spectrosc.* **1991**, *145*, 315.
(10) Duck-Lae, J.; Merer, A. J.; Clouthier, D. J. *J. Mol. Spectrosc.* **1999**, *197*, 68.
(11) Van Santen, R. A.; Neurock, M. *Catal. Rev. Sci. Eng.* **1995**, *37*, 557.
(12) Fahmi, A.; Van Santen, R. A. *J. Phys. Chem.* **1996**, *100*, 5676.
(13) Siegbahn, P. E. M. *Adv. Chem. Phys.* **1996**, *93*, 333.
(14) Van Santen, R. A. In *Chemisorption and Reactivity on Supported Clusters and Thin films*; NATO ASI Series E: Applied Sciences; Lambert, R. M., Pacchioni, B., Eds.; Kluwer: Dordrecht, The Netherlands, 1997; Vol. 331, p 371.
(15) Paul, J. F.; Sautet, P. *Stud. Surf. Sci. Catal.* **1996**, *101*, 1253.
(16) Yokoyama, C.; Misono, M. *J. Catal*. **1994**, *150*, 9.
(17) Tanaka, T.; Okuhara, T.; Misono, M. *Appl. Catal. B* **1994**, *B4*, L1.
(18) Bethke, K. A.; Li, C.; Kung, M. C.; Yang, B.; Kung, H. H. *Catal. Lett.* **1995**, *31*, 287.
(19) Shimizu, K.; Shibata, J.; Yoshida, H.; Satsuma, A.; Hattori, T. *Appl. Catal. B* **2001**, *30*, 151.
(20) Meunier, F. C.; Zuzaniuk, V.; Breen, J. P.; Olsson, M.; Ross, J. R. H. *Catal. Today* **2000**, *59*, 287.
(21) Meunier, F. C.; Breen, J. P.; Zuzaniuk, V.; Olsson, M.; Ross, J. R. H. *J. Catal.* **1999**, *187*, 493.
(22) Shimizu, K.; Satsuma, A.; Hattori, T. *Appl. Catal. B* **2000**, *25*, 239.
(23) Rajh, T.; Chen, L. X.; Lukas, K.; Liu, T.; Thurnauer, M. C.; Tiede, D. M. *J. Phys. Chem. B* **2002**, *106*, 10543.
(24) Yu, Y.; Gao, H.; He, H. *Catal. Today* **2004**, *93*−*95*, 805.